Supporting Information:

Accessing the Accuracy of Density Functional Theory through Structure and Dynamics of the Water−Air Interface

Tatsuhiko Ohto,[1,#] Mayank Dodia,[2,#] Jianhang Xu,[3] Sho Imoto,[2] Fujie Tang,[3] Frederik Zysk[4], Thomas D. Kühne,[4] Yasuteru Shigeta,[5,6] Mischa Bonn,[2] Xifan Wu,[3] and Yuki Nagata[2,]*

1. Graduate School of Engineering Science, Osaka University, 1-3 Machikaneyama, Toyonaka, Osaka 560-8531, Japan
2. Max Planck Institute for Polymer Research, Ackermannweg 10, 55128 Mainz, Germany
3. Department of Physics, Temple University, Philadelphia, Pennsylvania 19122, USA
4. Dynamics of Condensed Matter and Center for Sustainable Systems Design, Chair of Theoretical Chemistry, University of Paderborn, Warburger Strasse 100, 33098 Paderborn, Germany
5. Graduate School of Pure and Applied Sciences, University of Tsukuba, Tennodai 1-1-1, Tsukuba, Ibaraki 305-8571, Japan
6. Center for Computational Sciences, University of Tsukuba, 1-1-1 Tennodai, Tsukuba, Ibaraki 305-8577, Japan

*Email: nagata@mpip-mainz.mpg.de

# These authors are equally contributed.

Contents:

1. Molecular Dynamics (MD) Simulation Protocols

1.1. Born-Oppenheimer MD (BOMD)

We performed BOMD simulations using the QUICKSTEP[1] method implemented in the CP2K code.[2] We used the PBE,[3] BLYP,[4,5] revPBE[3,6] generalized gradient approximation (GGA) exchange-correlation (XC) functionals, M06-L[7] and B97M-rV[8] meta-GGA XC functionals, and B3LYP,[5,9–11] revPBE0,[3,6,12] and HSE06[13,14] hybrid-GGA XC functionals with the auxiliary density matrix method (ADMM).[15] M06-L, revPBE0, HSE06, B3LYP functionals are also combined with empirical van der Waals (vdW) correction scheme using Grimme's D3(0)[16] correction. Furthermore, we examined the effect of ADMM on the structure and dynamics of interfacial water at the revPBE0-D3(0) hybrid-GGA level of theory.

We have used the mixed Gaussian and plane wave approach as implemented in the CP2K code.[2] The TZV2P basis set which is constructed using triple-ζ valance Gaussian basis with two sets of polarization functions was used for all BOMD simulations. For BOMD simulation with the hybrid-GGA functionals, we have utilized the ADMM method,[15] which requires an auxiliary basis (in addition to the primary TZV2P basis) to approximate the Hartree-Fock exchange energy. We used the FIT3 basis set, which uses three gaussian exponents for each valance orbital. To examine the effect of ADMM, we ran the simulation at the revPBE0-D3(0) hybrid-GGA level of theory without the ADMM, in addition to the revPBE0-D3(0) BOMD simulation with the ADMM. We set the plane wave density cutoff of 320 Ry for all the BOMD simulations, except the M06-L-D3(0) calculation; For the M06-L-D3(0), we used a cutoff of 1200 Ry, as M06-L functional requires a finer integration grid.[17] Norm-conserving Goedecker-Teter-Hutter pseudopotentials[18,19] were used to describe the core electrons. We used the grid

interpolation scheme for electron density[1] using the keyword options XC_SMOOTH_RHO NN50 and XC_DERIV SPLINE2_SMOOTH. D_2O was used instead of H_2O, and the time step was set to 0.5 fs. All simulations were performed at 300 K in *NVT* ensemble with the thermostat of the canonical sampling through velocity rescaling method.[20] We used 160 D_2O molecules in simulation cell $(L_x,L_y,L_z) = (16.63\ \text{Å}, 16.63\ \text{Å}, 44.10\ \text{Å})$, where the water-air interface is parallel to *xy* plane and the surface normal forms the *z*-axis. The cutoff radius of the vdW interactions was set to 10 Å. We ran 10 independent simulations from previously generated configurations from the simulation at the revPBE-D3(0) level of theory.[21] 16 ps MD trajectory was generated after 5 ps equilibration run. Configurations were captured at every 10-step and were used for analysis. The length of the trajectories were total ≥ 500 ps for BLYP, BLYP-D2, BLYP-D3(0), BLYP-D3(BJ), PBE, PBE-D2, PBE-D3(0), PBE-D3(BJ), revPBE-D3(0) and revPBE-D3(BJ) GGA functionals, ≥ 150 ps for PBE-D3m(BJ), PBE-DRSLL, PBE-rVV10, optB88-DRSLL, revPBE-D2, revPBE-DRSLL, revPBE-rvv10 GGA functionals, M06-L-D3(0), B97M-rV meta-GGA functionals, B3LYP-D3(0), HSE06-D3(0), revPBE0-D3(0) hybrid-GGA functionals, and 160 ps for revPBE-D3(0) hybrid-functionals without ADMM. For the SCAN meta-GGA functional, we obtained 56 ps trajectory.

1.1.1. **revPBE0 Hybrid Functional**

The exchange correlation energy for the revPBE0 functional can be defined as:

$$E_{\text{XC}}^{\text{revPBE}} = a_0 E_{\text{X}}^{\text{Exact}} + (1 - a_0) E_{\text{X}}^{\text{revPBE}} + E_{\text{C}}^{\text{PBE}}, \tag{S1}$$

where $E_{\text{X}}^{\text{revPBE}}$ and $E_{\text{C}}^{\text{PBE}}$ are the revPBE exchange and PBE correlation energies

respectively. The contribution of the exact exchange a_0 was set to 0.25.[12]

1.1.2. **HSE06 Hybrid Functional**

The HSE06 functional is a range separated functional replaces the long-range exact exchange interaction with PBE exchange functional. The total exchange correlation energy can be written as:

$$E_{\mathrm{XC}}^{\mathrm{HSE06}} = a_0 E_{\mathrm{X}}^{\mathrm{Exact,SR}}(\mu) + (1 - a_0) E_{\mathrm{X}}^{\mathrm{PBE,SR}}(\mu) + E_{\mathrm{X}}^{\mathrm{PBE,LR}}(\mu) + E_{\mathrm{C}}^{\mathrm{PBE}}, \quad \text{(S2)}$$

The exchange energy is separated into long-range and short-range components, labeled LR and SR respectively. The correlation energy is provided by the PBE correlation functionals. While parameter a_0 controls the exact exchange contribution to the exchange energy, parameter μ defines the range-separation. We used a_0= 0.25 and μ = 0.11.[13,14]

1.2. Car-Parrinello MD (CPMD)

Due to a problem in the wave function optimization with the SCAN functional in low electron density region such as the water-air interface with CP2K code,[22] one cannot perform the BOMD, as BOMD requires the wave function optimization for each step, which in contrast, is not required by CPMD due to its use of the fictious mass.[23] Note that the BOMD simulation with SCAN functional can be conducted for the bulk water with the CP2K code.[24] As such, we performed Car-Parrinello-type MD simulations[23] for the SCAN meta-GGA functional with the Quantum Espresso code.[25,26] We used 128 D_2O molecules in simulation cell $(L_x,L_y,L_z) = (12.44\ \text{Å}, 12.44\ \text{Å}, 50.00\ \text{Å})$. We used the Hamann-Schlüter-Chiang-Vanderbilt pseudopotentials[27,28] generated for PBE with plane wave cutoff of 85 Ry and a time step of 2 au (0.0484 fs). The simulation was performed at 300 K in *NVT* ensemble with the Nose-Hoover chain thermostat.[29,30] The fictitious mass

of electrons was set at 100 au.[31,32] The 56 ps FPMD trajectory was generated after 5 ps equilibration run. Note that the very similar results of the BOMD with CP2K and CPMD with Quantum Espresso were reported in Ref. 33.

1.3. POLI2VS Force Field MD

We performed the force field MD simulation with the POLI2VS model.[34] We prepared the two setups; for one setup 160 D_2O molecules were inserted in the simulation cell (L_x, L_y,L_z) = (16.63 Å,16.63 Å,44.10 Å), and for the other 128 D_2O molecules were inserted in simulation cell (L_x,L_y,L_z) = (12.44 Å,12.44 Å,50.00 Å). These setups correspond to the simulations of BOMD and CPMD. Both simulations used a 0.4 fs time step and the temperature was set to 300 K by using the Nosé–Hoover chain thermostat[29,30] in the *NVT* ensemble. The charge-charge, charge-dipole and dipole-dipole interactions were evaluated using Ewald summation, whereas quadrapole interactions were curtailed at 6 Å for 128 D_2O system and 8.3 Å for 160-D_2O system, respectively. We first ran 1 ns MD simulation for equilibration and then we obtained 3 ns for production run which was used for analysis. Trajectory was recorded every 20 steps for 128 D_2O system and 1000 steps for 160 D_2O system, respectively. Table S1 shows the comparison of bulk and interfacial water parameters for the simulations.

2. Target Quantities

2.1. Density Profile of Interfacial Water

The bulk water density ρ_0 (at zero pressure), the z-coordinate of the Gibbs dividing surface z_G, and the interfacial thickness parameter δ can be calculated by fitting the density profile in the water slab system with the hyperbolic tangent function $\rho(z)$ along the surface

normal (z-axis):

$$\rho(z) = \frac{\rho_0}{2}\left(1 - \tanh\left(-\frac{|z| - z_G}{\delta}\right)\right), \tag{S3}$$

For this calculation, the center of mass of the water slab was set at the origin of the z-axis and the deuterium atoms in D_2O were replaced by hydrogen atoms. It has been confirmed from the MD simulation with the POLI2VS force field model that ρ_0 calculated in the slab model (0.989±0.001 g/cm^3) is very close to that calculated in the *NPT* ensemble (0.993±0.001 g/cm^3).[34]

2.2. Radial Distribution Function (RDF)

We calculated the oxygen-oxygen radial distribution function (RDF), $g_{OO}(r)$, for the selected water molecules whose oxygen atoms were in the region $|z| \leq$ 1.35 Å (bulk region) of the slab model. The RDF was calculated based on the computed ρ_0 obtained via Eq. S3. The resolution of the RDF, Δr, was set to 0.1 Å. The results are shown in Figure S1.

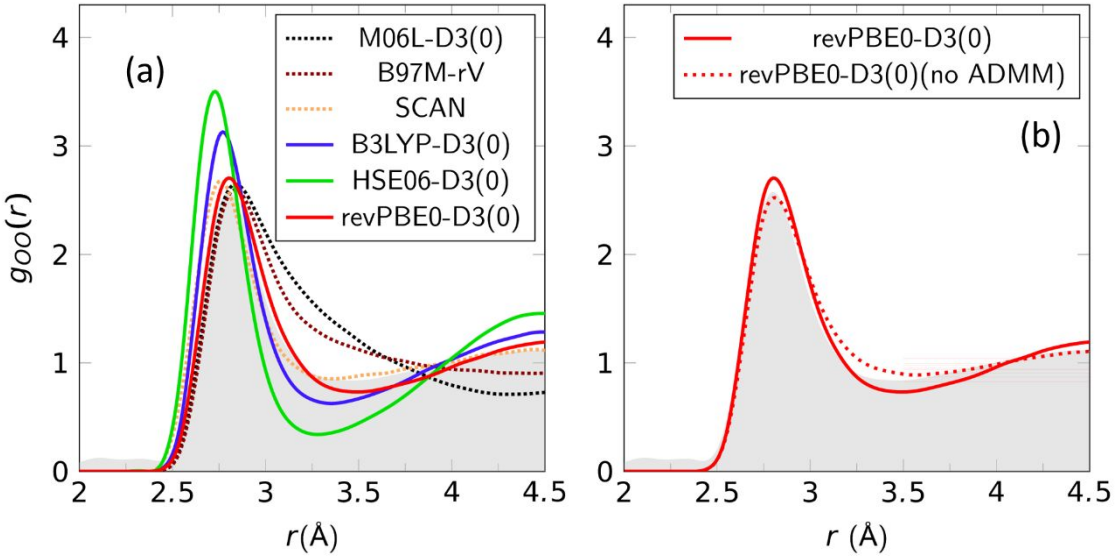

Figure S1: Oxygen-oxygen RDF of water simulated in the DFT-MD simulation with (a) meta-GGA and hybrid-GGA XC functionals, and (b) revPBE0-D3(0) functional with and without ADMM. The shaded area represent the experimental data from X-ray diffraction measurements.[35]

2.3. Fraction of Interfacial Water Molecules with Free O-D Group and Angle of Free O-D Group

A "free" O-D group of the D_2O molecule at the interface is defined as follows; the distance between its oxygen atom and an oxygen atom of any other water molecule (O⋯O distance) is larger than 3.5 Å and the D-O⋯O angle is greater than 50°.[36] Otherwise, an O-D group is defined as being hydrogen-bonded. The fraction of the D_2O molecule having free O-D groups is calculated as the sum of the DA and DAA fractions in the interfacial region of the slab system as follows:[37]

$$z_G - 3.11\ \text{Å} \leq |z| \leq z_G + 3.11\ \text{Å}. \tag{S4}$$

The fraction of the free O-D group estimated from the POLI2VS force field model is 28%, which is in good agreement with sum-frequency generation (SFG) spectroscopy measurements of 20-25%.[37,38] Thus, we can use 28 % as the reference value. It is also possible to calculate the averaged angle $\langle\theta\rangle$, formed by the free O-D groups and the surface normal. $\langle\theta\rangle$ can be estimated using polarization-dependent SFG spectroscopy.[39–45]

2.4. Lifetime of Free O-D Group

We calculated the lifetime of the free O-D group using the time correlation function

$$C(t) = \frac{\left\langle \prod_0^t h(t') \right\rangle}{\langle h(0) \rangle}, \tag{S5}$$

where $h(t)$ is defined as 1 when an O-D group is free at time t, otherwise 0. Within the time region 0-5 ps, $C(t)$ can be fitted with a double exponential form[46]

$$C(t) = ae^{-\left(\frac{t}{\tau_f}\right)} + be^{-\left(\frac{t}{\tau_s}\right)} + c, \tag{S6}$$

where a, b and c are the fitting coefficients. τ_f and τ_s are the fast and slow components of the time constants, respectively. τ_f is governed by the librational motion of water, while τ_s is governed by the motion that the free O-D group rotates and forms a hydrogen bond with another water molecule at the water-air interface. These time constants can be probed using time resolved SFG spectroscopy,[47–49] although the lifetime of the free O-H group has been obtained so far.[49] Since the POLI2VS simulation of H_2O agrees with the experimental data for H_2O,[36] we used the POLI2VS data of D_2O as the reference value. The time correlation functions are shown in Figure S2.

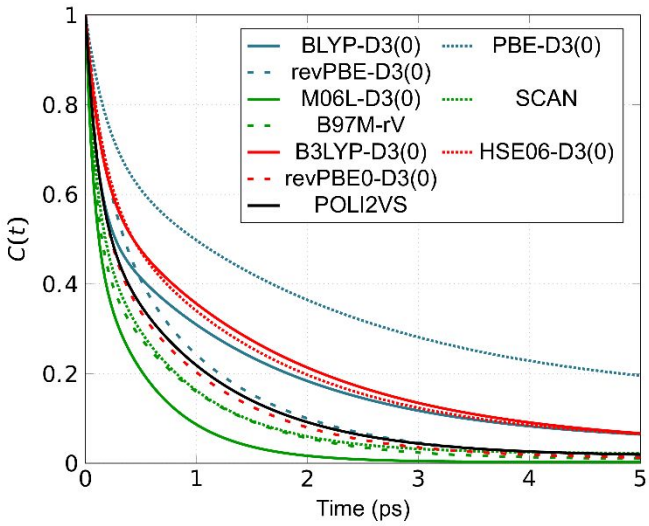

Figure S2: Time correlation functions of the free O-D group of the interfacial water molecules.

3. Complete Dataset for MD Simulations

In Table S1, we show all data obtained from DFT-MD simulations, including data from our previous papers.[21,50] The data used for reference are marked in shadow.

Table S1 : Bulk and interfacial water data using various DFT+vdW methods

	revPBE					PBE					optB88-DRSLL
	None	D2	D3(0)	D3(BJ)	DRSLL	rVV10	None	D2	D3(0)	D3(BJ)	D3m(BJ)	DRSLL	rVV10	
ρ (g/cm^3)	0.69	0.94	0.94	0.93	0.93	1.06	0.91	1.02	1.03	0.99	1.00	1.12	1.03	1.06
z_G (Å)	12.5	9.2	9.18	9.30	9.31	8.15	9.50	8.43	8.44	8.71	8.63	7.70	8.37	8.13
δ (Å)	2.06	1.06	1.17	1.12	1.05	1.03	1.08	1.06	1.01	1.04	1.02	0.81	0.96	1.01
DA(%)	27	12	11	14	19	9	12.3	7	8	8	9	6	7	7
DAA(%)	11	14	13	14	17	13	15	12	13	14	13	14	13	13
DDA(%)	13	18	17	18	19	17	17	17	17	17	17	17	17	16
Free OH (%)	38	26	24	28	35	23	27	19	21	22	22	20	19	20
<ϑ> (deg)	76	65	66	64	72	56	54	51	53	50	55	57	48	52
τ_f (ps)	0.19	0.12	0.11	0.15	0.10	0.13	0.19	0.16	0.15	0.18	0.17	0.09	0.21	0.15
τ_s (ps)	1.05	1.03	1.06	1.28	0.51	1.43	2.18	1.99	1.87	2.16	1.86	0.98	2.51	1.57
h_{max}	2.74	2.96	2.72	3.15	2.19	2.95	3.67	3.62	3.44	3.80	3.69	2.55	3.72	3.14
r_{max} (Å)	2.86	2.78	2.81	2.77	2.92	2.74	2.75	2.71	2.72	2.71	2.71	2.82	2.70	2.75
h_{min}	0.46	0.57	0.69	0.41	-	0.67	0.18	0.31	0.36	0.18	0.21	-	0.23	0.59
r_{min} (Å)	3.61	3.41	3.46	3.36	-	3.23	3.36	3.25	3.26	3.27	3.28	-	3.24	3.25

	BLYP				M06-L-D3(0)	SCAN	B97MrV	B3LYP-D3(0)	HSE06-D3(0)	revPBE-D3(0)	revPBE0-D3(0) (no ADMM)	POLI2VS Reference		Experimental Reference
	none	D2	D3(0)	D3(BJ)								160 D_2O	128 D_2O	
ρ (g/cm^3)	0.79	1.01	1.05	0.96	1.25	1.06	1.11	0.98	0.98	0.92	0.98	0.99	0.98	1.00
z_G (Å)	10.8	8.57	8.20	9.01	6.96	11.6	7.78	8.79	8.85	9.36	8.81	8.76	12.55	
δ (Å)	1.38	1.00	1.10	0.98	0.96	0.92	1.04	1.17	1.09	1.41	1.14	1.29	1.14	
DA(%)	19	7	7	9	6	9	7	10	13	15	11	12	12	
DAA(%)	14	11	12	13	15	15	14	13	14	14	14	16	16	
DDA(%)	15	16	16	17	15	18	16	16	16	17	17	17	17	
Free OH (%)	33	18	19	22	21	24	21	23	26	30	25	28	28	~20-25
<ϑ> (deg)	62	54	56	54	57	60	60	55	57	66	64	61	62	63
τ_f (ps)	0.20	0.12	0.10	0.15	0.07	0.09	0.08	0.14	0.16	0.12	0.10	0.11	0.20	
τ_s (ps)	1.92	1.72	1.56	1.94	0.57	0.77	0.86	1.69	1.51	0.99	1.00	1.02	1.00	1.01
h_{max}	3.41	3.47	2.81	3.60	2.65	2.66	2.59	3.13	3.50	2.70	2.52	2.73	2.66	2.58
r_{max} (Å)	2.81	2.75	2.78	2.76	2.84	2.76	2.84	2.77	2.73	2.80	2.81	2.78	2.80	2.80
h_{min}	0.25	0.46	0.90	0.27	-	0.88	-	0.60	0.34	0.73	0.89	0.83	0.83	0.84
r_{min} (Å)	3.47	3.33	3.41	3.32	-	3.41	-	3.37	3.28	3.49	3.56	3.43	3.47	3.47

4. Ranking Procedure

We ranked the performance of various GGA, meta-GGA, and hybrid-GGA XC functionals by using the following equation:

$$\kappa_i^j = \frac{\left|\chi_i^j - \chi_i^{\mathrm{Ref}}\right|}{\sigma_i}, \tag{S7}$$

where κ_i^j is the score of the DFT method j for the calculated property i=[ρ, interfacial free O-D fraction, $\langle\theta\rangle$, τ_s, $g_{\mathrm{OO}}(r)$]. χ_i^j denotes the value of the quantity i computed with the method j, χ_i^{Ref} is the reference value of the quantity i and σ_i is the standard deviation of quantity i for all DFT XC-functionals in Table 1. The ranking for $g_{\mathrm{OO}}(r)$ for the method j was calculated using the average error score for individual components of $g_{\mathrm{OO}}(r)$, i.e., the set [h_{max}, r_{max}, h_{min}, r_{min}]. Since h_{min} and r_{min} could not be defined for B97M-rV and M06-L-D3(0) meta-GGA functionals, the error score for the RDF data were evaluated by taking the average score of h_{max} and r_{max} for these functionals. Using the above expression, a smaller value κ_i^j implies better performance by method j for quantity i. For all values for BOMD simulations except density (χ_ρ^{Ref} = 1.00 g/cm^3) and $g_{\mathrm{OO}}(r)$ data from X-ray diffraction measurements,[35] the 160 D_2O POLI2VS MD simulations results have been taken as the reference values. For SCAN functional, reference values were set to 128 D_2O POLI2VS simulation results, with χ_ρ^{Ref} = 1.00 g/cm^3 and experimentally measured $g_{\mathrm{OO}}(r)$.[35] The resultant ranking is listed in Table S2.

Table S2: Score of various DFT functionals for bulk and interfacial data.

	revPBE						PBE							optB88-DRSLL
	None	D2	D3(0)	D3(BJ)	DRSLL	rVV10	None	D2	D3(0)	D3(BJ)	D3m(BJ)	DRSLL	rVV10	
ρ	2.88	0.59	0.55	0.68	0.68	0.58	0.86	0.21	0.27	0.06	0.02	1.12	0.31	0.58
δ	3.27	0.97	0.49	0.74	1.00	1.11	0.89	0.99	1.17	1.06	1.17	2.04	1.41	1.20
fraction	1.98	0.36	0.70	0.06	1.43	1.02	0.17	1.65	1.38	1.10	1.18	1.59	1.63	1.51
$\langle\vartheta\rangle$	2.14	0.47	0.59	0.41	1.56	0.78	1.07	1.60	1.19	1.62	1.02	0.73	1.90	1.35
τ_s	0.06	0.02	0.07	0.48	0.95	0.86	2.18	1.81	1.59	2.14	1.57	0.04	2.62	1.03
h_{max}	0.35	0.81	0.30	1.21	0.84	0.81	2.32	2.23	1.85	2.60	2.38	0.08	2.45	1.21
r_{max}	1.11	0.37	0.19	0.56	2.22	1.11	0.93	1.67	1.48	1.67	1.67	0.37	1.85	0.93
h_{min}	1.56	1.12	0.60	1.76	-	-	2.72	2.18	1.97	2.74	2.61	-	2.52	1.03
r_{min}	1.28	0.55	0.09	1.01	-	-	1.01	2.02	1.93	1.83	1.74	-	2.11	2.02
Final score	2.28	0.62	0.54	0.70	1.43	1.06	1.38	1.66	1.48	1.64	1.41	1.15	2.02	1.39

	BLYP				M06-L-D3(0)	SCAN	B97M-rV	B3LYP-D3(0)	HSE06-D3(0)	revPBE0-D3(0)	revPBE0-D3(0) (no ADMM)
	None	D2	D3(0)	D3(BJ)							
ρ	1.93	0.07	0.51	0.39	2.29	0.60	1.06	0.14	0.21	0.71	0.18
δ	0.40	1.23	0.83	1.32	1.40	0.91	1.10	0.49	0.85	0.50	0.64
fraction	0.92	1.87	1.74	1.17	1.26	0.61	1.36	0.99	0.32	0.32	0.56
$\langle\vartheta\rangle$	0.10	1.05	0.77	1.07	0.70	0.24	0.26	0.93	0.66	0.68	0.37
τ_s	1.68	1.30	1.00	1.72	0.84	0.43	0.30	1.26	0.92	0.06	0.04
h_{max}	1.78	1.91	0.51	2.18	0.16	0.00	0.04	1.18	1.96	0.27	0.11
r_{max}	0.19	0.93	0.37	0.74	0.74	0.74	0.74	0.56	1.30	0.00	0.19
h_{min}	2.43	1.56	0.26	2.35	-	0.24	-	0.96	2.05	0.44	0.21
r_{min}	0.00	1.28	0.55	1.38	-	0.55	-	0.92	1.74	0.18	0.83
Final score	1.22	1.39	1.06	1.47	1.39	0.64	0.89	0.94	0.94	0.50	0.43

5. Effect of ADMM

ADMM[15] reduces the computational cost for the calculation of the exact-exchange term by introducing the auxiliary density calculated using an auxiliary basis set. Table S1 shows that the ADMM does not affect the free O-D fraction and angle, while the density of water is ~7% higher without ADMM than with ADMM. This is consistent with Ref. 51. For the interfacial water, one can see the difference in the fraction of the water molecules with free O-D groups. This indicates that the ADMM affects the water structure in a non-negligible manner. Thus, accurate implementation of ADMM at a computationally reasonable cost is highly required.

6. Relative Computational Cost

The relative computational cost for the DFT XC functionals in provided in Table S3. We chose to compare the time needed for 0.5 fs for different XC functionals. The average error for time is 0.78 s. All the BOMD values have been evaluated using a single Intel Xeon E5-2630-v4 node. Relative computational cost for SCAN with Quantum Espresso code was estimated through the comparison with the cost for revPBE0-D3(0) without ADMM with CP2K code using the 16 Intel Xeon Gold 6126 nodes.

Table S3. Relative computational cost for the DFT XC functionals. DFT methods written in red, blue, and green are at the GGA, meta-GGA, and hybrid-GGA DFT levels of theory, respectively. The average error for time is 0.78 s.

Method	Time(s)	Cost	Method	Time(s)	Cost
revPBE	30	0.76	optB88-DRSLL	118	2.99
revPBE-D2	36	0.91	BLYP	29	0.73
revPBE-D3(0)	40	1.00	BLYP-D2	33	0.84
revPBE-D3(BJ)	47	1.19	BLYP-D3(0)	42	1.05
revPBE-DRSLL	116	2.91	BLYP-D3(BJ)	47	1.19
revPBE-rVV10	118	2.98	M06-L-D3(0)	174	4.39
PBE	33	0.83	SCAN	(8759)	(221)
PBE-D2	35	0.88	B97M-rV	149	3.77
PBE-D3(0)	42	1.07	HSE06-D3(0)	149	3.76
PBE-D3(BJ)	49	1.24	B3LYP-D3(0)	151	3.82
PBE-D3(mBJ)	42	1.06	revPBE0-D3(0)	155	3.90
PBE-DRSLL	119	3.00	revPBE0-D3(0) no ADMM	561	14.1
PBE-rVV10	118	2.97			

7. Simulation Protocols of SFG Spectra

To simulate sum-frequency generation spectra from density functional theory-based molecular dynamics (DFT-MD) trajectories, we used the surface-specific velocity-velocity correlation function (ssVVCF) algorithm,[52] where the resonant part of the SFG response function, $\chi_{xxz}^{(2),R}(\omega)$ can be written as:

$$\chi_{xxz}^{(2),R}(\omega) = \frac{Q(\omega)\mu'(\omega)\alpha'(\omega)}{i\omega^2}\chi_{xxz}^{ssVVAF}(\omega), \quad \text{(S8)}$$

$$\chi_{xxz}^{ssVVCF}(\omega) = \int_0^\infty dt e^{-i\omega t}\left\langle \sum_{i,j} g_{ds}(z_i(0))\dot{r}_{z,i}^{OD}(0)\frac{\dot{\vec{r}}_j^{OD}(t)\cdot\vec{r}_j^{OD}(t)}{|\vec{r}_j^{OD}(t)|}\right\rangle, \quad \text{(S9)}$$

where $z_i(t)$ is the z-coordinate of the ith oxygen atom at time t, and $g_{ds}(z_i)$ is the function for the dividing surface to selectively extract the vibrational responses of D_2O molecules near the interface given by:

$$g_{ds}(z_i) = \begin{cases} -1 & \text{for} \quad z_i < -2\ \text{Å} \\ 0 & \text{for} \quad -2\ \text{Å} \le z_i < 2\ \text{Å} \\ 1 & \text{for} \quad 2\ \text{Å} \le z_i \end{cases}. \quad \text{(S10)}$$

With this $g_{ds}(z_i)$ function, we can include the contributions from both surfaces of the water slab into the correlation function and exclude the contribution from the bulk. $Q(\omega)$ is the quantum correction factor given by:[53]

$$Q(\omega) = \frac{\beta\hbar\omega}{1 - \exp(-\beta\hbar\omega)}, \quad \text{(S11)}$$

where $\beta = 1/kT$ is the inverse temperature.

In this study, we consider the case that the O-D stretch chromophores are decoupled from the other O-D chromophores. This corresponds to the situation of isotopically diluted water (HOD in D_2O). When the O-D stretch chromophores are isolated, the cross-correlation term in Equation (S9) is zero and thus, is reduced to the surface-specific autocorrelation function (ssVVAF) as:

$$\chi_{xxz}^{ssVVAF}(\omega) = \int_0^T dt e^{-i\omega t} f(t)\left\langle \sum_i g_{ds}(z_i(0))\dot{r}_{z,i}^{OD}(0)\frac{\dot{\vec{r}}_i^{OD}(t)\cdot\vec{r}_i^{OD}(t)}{|\vec{r}_i^{OD}(t)|}\right\rangle, \quad \text{(S12)}$$

where T is the length of the time correlation function and $f(t)$ is the window function for the Fourier transformation. Here, we set T = 1 ps for all the DFT-MD trajectories except SCAN which used T = 0.5 ps. We used the Hann window function for $f(t)$. The induced dipole moment due to the surrounding water molecules (solvation effects) are included through the frequency dependent transition dipole moment (μ'(ω)) and polarizability

(α'(ω)):[54,55]

$$\mu'(\omega) \equiv \left(1.377 + \frac{53.03(2745.8 - \omega)}{4870.3}\right)\mu^0, \quad \text{(S13)}$$

$$\alpha'(\omega) \equiv \left(1.271 + \frac{5.287(2745.8 - \omega)}{4870.3}\right)\alpha^0, \quad \text{(S14)}$$

where the unit of ω is cm^{-1}.

It is also known that the nuclear quantum effect induces a redshift of the O-H(D) stretching frequency.[56] The factor of 0.96[48,57,58] or the 123 cm^{-1} red shift (175 cm^{-1} red-shift for the O-H stretch mode[59]) were used for correcting the frequency. In this study, we used scale factor of 0.96 for correcting the vibrational frequency of the O-D stretch mode. Note that the quantum correction factor $Q(\omega)$ was calculated based on the scaled frequency. The same scaling factor and the quantum correction factors were also applied for POLI2VS data of HOD.

8. Full Width at Half Maximum (FWHM) of the Negative SFG Feature

The FWHM of a negative SFG feature which originates from the hydrogen-bonded O-D groups was measured from the points on the *y*-axis which are half of the maximum amplitude of the peak. The obtained FWHM data are listed in Table S4.

Table S4. FWHM values of the negative SFG peaks. Error bars represent 95% confidence interval. [a]Ref. 60. [b]Ref. 61

Method	FWHM (cm^{-1})	Method	FWHM (cm^{-1})
revPBE	199 ± 17	BLYP	189 ± 12
revPBE-D2	189 ± 14	BLYP-D2	189 ± 12
revPBE-D3(0)	160 ± 14	BLYP-D3(0)	189 ± 13
revPBE-D3(BJ)	197 ± 20	BLYP-D3(BJ)	179 ± 9
revPBE-DRSLL	115 ± 16	M06-L-D3(0)	126 ± 19
revPBE-rVV10	207 ± 20	SCAN	238 ± 32
PBE	216 ± 22	B97M-rV	122 ± 10
PBE-D2	211 ± 13	HSE06-D3(0)	207 ± 33
PBE-D3(0)	223 ± 25	B3LYP-D3(0)	171 ± 22
PBE-D3(BJ)	201 ± 18	revPBE0-D3(0)	146 ± 10
PBE-D3(mBJ)	203 ± 20	revPBE0-D3(0) no ADMM	133 ± 20
PBE-DRSLL	181 ± 19	POLI2VS	124
PBE-rVV10	239 ± 28	Experiment (Tahara *et. al.*) [57]	128
optB88-DRSLL	189 ± 21	Experiment (Tian *et.al.*) [58]	129

9. Nuclear Quantum Effects

Nuclear quantum effects are known to be essential to describe water properties. To investigate the impact of nuclear quantum effects on the target quantities calculated in this work, we performed classical MD and quantum mechanical partially adiabatic centroid MD (PA-CMD) simulations using the q-TIP4P/F[62] water model, augmented by the explicit three-body (E3B) interactions by Skinner and coworkers[63]. The simulated water slab consisted of 216 heavy water molecules in an orthorhombic simulation cell (L_x,L_y,L_z) = (18.64 Å, 18.64 Å, 55.93 Å). Short-range interactions were truncated at 10 Å, while the Ewald summation scheme was employed to treat the long-range electrostatic interactions. To explicitly include nuclear quantum effects in a computationally efficient way, the ring-polymer contraction scheme of Manolopoulos and coworkers was used with a cutoff value of 5 Å in order to reduce the electrostatic potential energy and force calculations to a single Ewald sum, thereby accelerating the calculation[62]. More precisely, 32 ring-polymer beads were used to converge all relevant properties[64], whereas the computational expensive part of the electrostatic interactions were contracted to the centroid only. In all simulations, using a discretized time-step of 0.25 fs, the system was first equilibrated for 250 ps in the canonical ensemble, before microcanonical ensemble averages were computed over the following 250 ps.

Table S5 lists the calculated properties for both classical and quantum simulations. The trend for τ_s for classical and quantum simulations is similar to the trend for the water reorientation dynamics reported by Paesani *et. al.*[63] and Wilkins *et al.*[64]. Overall, the nuclear quantum effects have quite limited effects of the free O-D angle and fractions.

Table S5. Bulk and interfacial properties for q-TIP4P/F model using classical and quantum simulations.

	q-tip4p/f	
	Classical	Quantum
ρ (g/cm^3)	1.00	1.01
h_{max}	3.48	3.58
r_{max} ( )	2.76	2.76
h_{min}	0.59	0.57
r_{min} ( )	3.27	3.25
δ ( )	1.24	1.23
Free O-D (%)	24	23
$\langle\vartheta\rangle$ (deg)	58	58
τ_s (ps)	0.68	0.76

References

(1) Vandevondele, J.; Krack, M.; Mohamed, F.; Parrinello, M.; Chassaing, T.; Hutter, J. Quickstep: Fast and Accurate Density Functional Calculations Using a Mixed Gaussian and Plane Waves Approach. *Comput. Phys. Commun.* **2005**, *167*, 103–128.

(2) Hutter, J.; Iannuzzi, M.; Schiffmann, F.; Vandevondele, J. CP2K: Atomistic Simulations of Condensed Matter Systems. *Wiley Interdiscip. Rev. Comput. Mol. Sci.* **2014**, *4*, 15–25.

(3) Perdew, J. P.; Burke, K.; Ernzerhof, M. Generalized Gradient Approximation Made Simple. *Phys. Rev. Lett.* **1996**, *77*, 3865–3868.

(4) Becke, A. D. Density-Functional Exchange-Energy Approximation with Correct Asymptotic Behavior. *Phys. Rev. A* **1988**, *38*, 3098–3100.

(5) Lee, C.; Yang, W.; Parr, R. G. Development of the Colle-Salvetti Correlation-Energy Formula into a Functional of the Electron Density. *Phys. Rev. B* **1988**, *37*, 785–789.

(6) Zhang, Y.; Yang, W. Comment on "Generalized Gradient Approximation Made Simple." *Phys. Rev. Lett.* **1998**, *80*, 890.

(7) Zhao, Y.; Truhlar, D. G. A New Local Density Functional for Main-Group Thermochemistry, Transition Metal Bonding, Thermochemical Kinetics, and Noncovalent Interactions. *J. Chem. Phys.* **2006**, *125*, 194101.

(8) Mardirossian, N.; Head-Gordon, M. Mapping the Genome of Meta-Generalized

Gradient Approximation Density Functionals: The Search for B97M-V. *J. Chem. Phys.* **2015**, *142*, 074111.

(9) Vosko, S. H.; Wilk, L.; Nusair, M. Accurate Spin-Dependent Electron Liquid Correlation Energies for Local Spin Density Calculations: A Critical Analysis. *Can. J. Phys.* **1980**, *58*, 1200–1211.

(10) Stephens, P. J.; Devlin, F. J.; Chabalowski, C. F.; Frisch, M. J. Ab Initio Calculation of Vibrational Absorption and Circular Dichroism Spectra Using Density Functional Force Fields. *J. Phys. Chem.* **1994**, *98*, 11623–11627.

(11) Becke, A. D. Density-Functional Thermochemistry. III. The Role of Exact Exchange. *J. Chem. Phys.* **1993**, *98*, 5648.

(12) Adamo, C.; Barone, V. Toward Reliable Density Functional Methods without Adjustable Parameters: The PBE0 Model. *J. Chem. Phys.* **1999**, *110*, 6158–6170.

(13) Heyd, J.; Scuseria, G. E.; Ernzerhof, M. Hybrid Functionals Based on a Screened Coulomb Potential. *J. Chem. Phys.* **2003**, *118*, 8207–8215.

(14) Krukau, A. V.; Vydrov, O. A.; Izmaylov, A. F.; Scuseria, G. E. Influence of the Exchange Screening Parameter on the Performance of Screened Hybrid Functionals. *J. Chem. Phys.* **2006**, *125*, 224106.

(15) Guidon, M.; Hutter, J.; Vandevondele, J. Auxiliary Density Matrix Methods for Hartree-Fock Exchange Calculations. *J. Chem. Theory Comput.* **2010**, *6*, 2348–2364.

(16) Grimme, S.; Antony, J.; Ehrlich, S.; Krieg, H. A Consistent and Accurate Ab Initio Parametrization of Density Functional Dispersion Correction (DFT-D) for the 94 Elements H-Pu. *J. Chem. Phys.* **2010**, *132*, 154104.

(17) Ruiz Pestana, L.; Mardirossian, N.; Head-Gordon, M.; Head-Gordon, T. Ab Initio Molecular Dynamics Simulations of Liquid Water Using High Quality Meta-GGA Functionals. *Chem. Sci.* **2017**, *8*, 3554–3565.

(18) Goedecker, S.; Teter, M.; Hutter, J. Separable Dual-Space Gaussian Pseudopotentials. *Phys. Rev. B* **1996**, *54*, 1703–1710.

(19) Krack, M. Pseudopotentials for H to Kr Optimized for Gradient-Corrected Exchange-Correlation Functionals. *Theor. Chem. Acc.* **2005**, *114*, 145–152.

(20) Bussi, G.; Donadio, D.; Parrinello, M. Canonical Sampling through Velocity Rescaling. *J. Chem. Phys.* **2007**, *126*, 014101.

(21) Ohto, T.; Dodia, M.; Imoto, S.; Nagata, Y. Structure and Dynamics of Water at the Water−Air Interface Using First-Principles Molecular Dynamics Simulations within Generalized Gradient Approximation. *J. Chem. Theory Comput.* **2019**, *15*, 595–602.

(22) Hutter, J. convergency problem using SCAN+rVV10.
(23) Car, R.; Parrinello, M. Unified Approach for Molecular Dynamics and Density-Functional Theory. *Phys. Rev. Lett.* **1985**, *55*, 2471–2474.
(24) Wiktor, J.; Ambrosio, F.; Pasquarello, A. Note: Assessment of the SCAN+rVV10 Functional for the Structure of Liquid Water. *J. Chem. Phys.* **2017**, *147*, 10–12.
(25) Giannozzi, P.; Baroni, S.; Bonini, N.; Calandra, M.; Car, R.; Cavazzoni, C.; Ceresoli, D.; Chiarotti, G. L.; Cococcioni, M.; Dabo, I.; et al. QUANTUM ESPRESSO: A Modular and Open-Source Software Project for Quantum Simulations of Materials. *J. Phys. Condens. Matter* **2009**, *21*, 395502.
(26) Giannozzi, P.; Andreussi, O.; Brumme, T.; Bunau, O.; Buongiorno Nardelli, M.; Calandra, M.; Car, R.; Cavazzoni, C.; Ceresoli, D.; Cococcioni, M.; et al. Advanced Capabilities for Materials Modelling with Quantum ESPRESSO. *J. Phys. Condens. Matter* **2017**, *29*, 465901.
(27) Hamann, D. R.; Schlüter, M.; Chiang, C. Norm-Conserving Pseudopotentials. *Phys. Rev. Lett.* **1979**, *43*, 1494–1497.
(28) Vanderbilt, D. Optimally Smooth Norm-Conserving Pseudopotentials. *Phys. Rev. B* **1985**, *32*, 8412–8415.
(29) Martyna, G. J.; Klein, M. L.; Tuckerman, M. Nosé–Hoover Chains: The Canonical Ensemble via Continuous Dynamics. *J. Chem. Phys.* **1992**, *97*, 2635–2643.
(30) Hoover, W. G. Canonical Dynamics: Equilibrium Phase-Space Distributions. *Phys. Rev. A* **1985**, *31*, 1695–1697.
(31) Kuo, I. F. W.; Mundy, C. J.; McGrath, M. J.; Siepmann, J. I. Time-Dependent Properties of Liquid Water: A Comparison of Car-Parrinello and Born-Oppenheimer Molecular Dynamics Simulations. *J. Chem. Theory Comput.* **2006**, *2*, 1274–1281.
(32) Chen, M.; Ko, H.-Y.; Remsing, R. C.; Calegari Andrade, M. F.; Santra, B.; Sun, Z.; Selloni, A.; Car, R.; Klein, M. L.; Perdew, J. P.; et al. Ab Initio Theory and Modeling of Water. *Proc. Natl. Acad. Sci. U. S. A.* **2017**, *114*, 10846–10851.
(33) Kuo, I.-F. W.; Mundy, C. J.; McGrath, M. J.; Siepmann, J. I.; VandeVondele, J.; Sprik, M.; Hutter, J.; Chen, B.; Klein, M. L.; Mohamed, F.; et al. Liquid Water from First Principles: Investigation of Different Sampling Approaches. *J. Phys. Chem. B* **2004**, *108*, 12990–12998.
(34) Hasegawa, T.; Tanimura, Y. A Polarizable Water Model for Intramolecular and Intermolecular Vibrational Spectroscopies. *J. Phys. Chem. B* **2011**, *115*, 5545–5553.
(35) Skinner, L. B.; Huang, C.; Schlesinger, D.; Pettersson, L. G. M.; Nilsson, A.;

Benmore, C. J. Benchmark Oxygen-Oxygen Pair-Distribution Function of Ambient Water from X-Ray Diffraction Measurements with a Wide Q-Range. *J. Chem. Phys.* **2013**, *138*, 074506.

(36) Tang, F.; Ohto, T.; Hasegawa, T.; Xie, W. J.; Xu, L.; Bonn, M.; Nagata, Y. Definition of Free O–H Groups of Water at the Air–Water Interface. *J. Chem. Theory Comput.* **2018**, *14*, 357–364.

(37) Du, Q.; Superfine, R.; Freysz, E.; Shen, Y. R. Vibrational Spectroscopy of Water at the Vapor/Water Interface. *Phys. Rev. Lett.* **1993**, *70*, 2313–2316.

(38) Du, Q.; Freysz, E.; Shen, Y. R. Surface Vibrational Spectroscopic Studies of Hydrogen Bonding and Hydrophobicity. *Science (80-.).* **1994**, *264*, 826–828.

(39) Gan, W.; Wu, D.; Zhang, Z.; Feng, R.; Wang, H. Polarization and Experimental Configuration Analyses of Sum Frequency Generation Vibrational Spectra, Structure, and Orientational Motion of the Air/Water Interface. *J. Chem. Phys.* **2006**, *124*, 114705.

(40) Feng, R.-R.; Guo, Y.; Wang, H.-F. Reorientation of the “Free OH” Group in the Top-Most Layer of Air/Water Interface of Sodium Fluoride Aqueous Solution Probed with Sum-Frequency Generation Vibrational Spectroscopy. *J. Chem. Phys.* **2014**, *141*, 18C507.

(41) Wei, X.; Miranda, P. B.; Zhang, C.; Shen, Y. R. Sum-Frequency Spectroscopic Studies of Ice Interfaces. *Phys. Rev. B* **2002**, *66*, 085401.

(42) Wei, X.; Shen, Y. R. Motional Effect in Surface Sum-Frequency Vibrational Spectroscopy. *Phys. Rev. Lett.* **2001**, *86*, 4799–4802.

(43) Rao, Y.; Tao, Y. S.; Wang, H. F. Quantitative Analysis of Orientational Order in the Molecular Monolayer by Surface Second Harmonic Generation. *J. Chem. Phys.* **2003**, *119*, 5226–5236.

(44) Wei, X.; Miranda, P. B.; Shen, Y. R. Surface Vibrational Spectroscopic Study of Surface Melting of Ice. *Phys. Rev. Lett.* **2001**, *86*, 1554–1557.

(45) Sun, S.; Tang, F.; Imoto, S.; Moberg, D. R.; Ohto, T.; Paesani, F.; Bonn, M.; Backus, E. H. G.; Nagata, Y. Orientational Distribution of Free O-H Groups of Interfacial Water Is Exponential. *Phys. Rev. Lett.* **2018**, *121*, 246101.

(46) Asbury, J. B.; Steinel, T.; Kwak, K.; Corcelli, S. A.; Lawrence, C. P.; Skinner, J. L.; Fayer, M. D. Dynamics of Water Probed with Vibrational Echo Correlation Spectroscopy. *J. Chem. Phys.* **2004**, *121*, 12431–12446.

(47) McGuire, J. A.; Shen, Y. R. Ultrafast Vibrational Dynamics at Water Interfaces. *Science (80-.).* **2006**, *313*, 1945–1948.

(48) Smit, W. J.; Tang, F.; Sánchez, M. A.; Backus, E. H. G.; Xu, L.; Hasegawa, T.;

Bonn, M.; Bakker, H. J.; Nagata, Y. Excess Hydrogen Bond at the Ice-Vapor Interface around 200 K. *Phys. Rev. Lett.* **2017**, *119*, 133003.

(49) Hsieh, C.-S.; Campen, R. K.; Okuno, M.; Backus, E. H. G.; Nagata, Y.; Bonn, M. Mechanism of Vibrational Energy Dissipation of Free OH Groups at the Air–Water Interface. *Proc. Natl. Acad. Sci. U.S.A.* **2013**, *110*, 18780–18785.

(50) Dodia, M.; Ohto, T.; Imoto, S.; Nagata, Y. Structure and Dynamics of Water at the Water–Air Interface Using First-Principles Molecular Dynamics Simulations. II. NonLocal vs Empirical van Der Waals Corrections. *J. Chem. Theory Comput.* **2019**, *15*, 3836–3843.

(51) Ben, M. Del; Hutter, J.; Vandevondele, J. Probing the Structural and Dynamical Properties of Liquid Water with Models Including Non-Local Electron Correlation. *J. Chem. Phys.* **2015**, *143*, 054506.

(52) Ohto, T.; Usui, K.; Hasegawa, T.; Bonn, M.; Nagata, Y. Toward Ab Initio Molecular Dynamics Modeling for Sum-Frequency Generation Spectra; an Efficient Algorithm Based on Surface-Specific Velocity-Velocity Correlation Function. *J. Chem. Phys.* **2015**, *143*, 124702.

(53) Berens, P. H. Molecular Dynamics and Spectra. I. Diatomic Rotation and Vibration. *J. Chem. Phys.* **1981**, *74*, 4872.

(54) Auer, B. M.; Skinner, J. L. IR and Raman Spectra of Liquid Water: Theory and Interpretation. *J. Chem. Phys.* **2008**, *128*, 224511.

(55) Corcelli, S. A.; Skinner, J. L. Infrared and Raman Line Shapes of Dilute HOD in Liquid H 2 O and D 2 O from 10 to 90 °C. *J. Phys. Chem. A* **2005**, *109*, 6154–6165.

(56) Marsalek, O.; Markland, T. E. Quantum Dynamics and Spectroscopy of Ab Initio Liquid Water: The Interplay of Nuclear and Electronic Quantum Effects. *J. Phys. Chem. Lett.* **2017**, *8*, 1545–1551.

(57) Nagata, Y.; Hasegawa, T.; Backus, E. H. G.; Usui, K.; Yoshimune, S.; Ohto, T.; Bonn, M. The Surface Roughness, but Not the Water Molecular Orientation Varies with Temperature at the Water–Air Interface. *Phys. Chem. Chem. Phys.* **2015**, *17*, 23559–23564.

(58) Smit, W. J.; Tang, F.; Nagata, Y.; Sánchez, M. A.; Hasegawa, T.; Backus, E. H. G.; Bonn, M.; Bakker, H. J. Observation and Identification of a New OH Stretch Vibrational Band at the Surface of Ice. *J. Phys. Chem. Lett.* **2017**, *8*, 3656–3660.

(59) Medders, G. R.; Paesani, F. Dissecting the Molecular Structure of the Air/Water Interface from Quantum Simulations of the Sum-Frequency Generation Spectrum. *J. Am. Chem. Soc.* **2016**, *138*, 3912–3919.

(60) Nihonyanagi, S.; Ishiyama, T.; Lee, T.-K.; Yamaguchi, S.; Bonn, M.; Morita, A.; Tahara, T. Unified Molecular View of the Air/Water Interface Based on Experimental and Theoretical χ(2) Spectra of an Isotopically Diluted Water Surface. *J. Am. Chem. Soc.* **2011**, *133*, 16875–16880.

(61) Xu, X.; Shen, Y. R.; Tian, C. Phase-Sensitive Sum Frequency Vibrational Spectroscopic Study of Air/Water Interfaces: H2O, D2O, and Diluted Isotopic Mixtures. *J. Chem. Phys.* **2019**, *150*, 144701.

(62) Habershon, S.; Markland, T. E.; Manolopoulos, D. E. Competing Quantum Effects in the Dynamics of a Flexible Water Model. *J. Chem. Phys.* **2009**, *131*, 024501.

(63) Paesani, F.; Yoo, S.; Bakker, H. J.; Xantheas, S. S. Nuclear Quantum Effects in the Reorientation of Water. *J. Phys. Chem. Lett.* **2010**, *1*, 2316–2321.

(64) Wilkins, D. M.; Manolopoulos, D. E.; Pipolo, S.; Laage, D.; Hynes, J. T. Nuclear Quantum Effects in Water Reorientation and Hydrogen-Bond Dynamics. *J. Phys. Chem. Lett.* **2017**, *8*, 2602–2607.